

Two-center interference in H_2^+ photoionization by electric dipole and quadrupole transitionsZhi Xu,¹ Jintai Liang^{1,*}, Kunlong Liu,² Marcelo F. Ciappina^{3,4,5,†}, Peixiang Lu,¹ and Yueming Zhou^{1,6,‡}¹*School of Physics and Wuhan National Laboratory for Optoelectronics, Huazhong University of Science and Technology, Wuhan 430074, China*²*School of Physical Sciences, Great Bay University, Dongguan 523000, China and Great Bay Institute for Advanced Study, Dongguan 523000, China*³*Department of Physics, Guangdong Technion—Israel Institute of Technology, 241 Daxue Road, Shantou, Guangdong 515063, China*⁴*Technion—Israel Institute of Technology, Haifa, 32000, Israel*⁵*Guangdong Provincial Key Laboratory of Materials and Technologies for Energy Conversion, Guangdong Technion—Israel Institute of Technology, 241 Daxue Road, Shantou, Guangdong 515063, China*⁶*Hubei Optical Fundamental Research Center, Wuhan 430074, China*

(Received 9 April 2024; accepted 2 July 2024; published 25 July 2024)

In molecular photoionization, the two-center interference is widely described within the electric dipole approximation, neglecting the electric quadrupole effect. By numerically solving the two-dimensional time-dependent Schrödinger equation beyond the dipole approximation and using perturbation theory, we demonstrate that the two-center interference structure induced by the electric quadrupole transition in the one-photon ionization of H_2^+ can be observed in the asymmetric photoelectron yield along the laser propagation direction. Compared with the dipole transition, the electron wave packets emitted from the two nuclei of the molecule due to the electric quadrupole transition exhibit an additional phase difference. This phase difference results in a distinct two-center interference structure compared to the dipole transition. Furthermore, an experimental scheme based on the reconstruction of attosecond beating by interference of two-photon transitions is proposed to reveal the two-center interference structure induced by the electric quadrupole transition. Our study provides a different perspective for investigating the nondipole effect in molecular photoionization.

DOI: [10.1103/PhysRevA.110.013124](https://doi.org/10.1103/PhysRevA.110.013124)**I. INTRODUCTION**

Photoionization is one of the most fundamental interaction processes in laser-matter interactions and plays a central role in ultrafast physics [1–7]. In photoionization, the electric dipole approximation is commonly used due to the mismatch between the spatial scale of electronic motion and the wavelength of light. Within this approximation, photon momentum, laser retardation, and the magnetic component of the laser field are neglected. This approximation generally holds well for the most commonly used near-infrared laser sources and intensities. However, in the short-wavelength regime and under intense high-intensity long-wavelength conditions [1], the scale of electronic motion becomes comparable to the light wavelength, and the electric dipole approximation breaks down.

Recently, with advances in detection technologies, the nondipole effect has become observable and has generated considerable interest. For instance, in strong-field atomic ionization with an IR field, the magnetic field component of the laser pulse plays a non-negligible role. The magnetic field induces an observable energy shift of the bound state [2,3] and significantly alters laser-induced electron-ion rescat-

tering [4–6,8]. Furthermore, the magnetic field complicates the partitioning of photon linear momentum between electrons and ions [9–12]. In atomic ionization by hard and soft x rays, the electric quadrupole effect becomes observable. It manifests as an asymmetric photoelectron angular distribution along the laser propagation direction [13–17]. This feature is significantly enhanced in autoionization [18], in the Cooper minimum [19], and in multiphoton resonant processes [20]. Moreover, it has been demonstrated that the electric quadrupole effect results in a distinct linear momentum transfer law in single-photon ionization [21,22].

Compared to atoms, the complicated structure of molecules introduces more intriguing scenarios. One of the simplest yet fundamentally important phenomena in molecular ionization is the two-center photoelectron interference, arising from the interference of electron wave packets (EWPs) emitted from the two centers of a diatomic molecule. This interference scheme was first proposed by Cohen and Fano [23] and has been experimentally observed in molecules such as H_2 [24–26], N_2 [27–29], and other dimers [30,31]. It has been utilized, for example, to study the onset of decoherence in a quantum system [24] and electron pair entanglement [26].

In recent years, there has been considerable interest in the interplay between two-center interference and the nondipole effect. For instance, the modification of two-center interference by magnetic-field effects has been observed in strong-field ionization [32,33]. In one-photon ionization, the

*Contact author: jintailiang@hust.edu.cn†Contact author: marcelo.ciappina@gtit.edu.cn‡Contact author: zhouymhust@hust.edu.cn

interference between the two centers leads to an oscillatory transfer of linear momentum from the photon to the electron as the photoelectron energy varies [34–36], significantly altering the photoelectron angular distribution along the laser propagation direction [37–41]. Interestingly, it has been demonstrated that two-center interference serves as a sensitive indicator of the effect of the finite speed of light in laser-molecule interactions [42]. Due to the finite speed of light, the emergence of a photoelectron wave from a two-center molecule is not simultaneous, introducing an additional phase difference in the ionization events from the two nuclei. This phase difference results in a shift in the interference fringes between the two centers, enabling the observation of zeptosecond-resolved birth time delays of the photoelectron [42–47]. In these studies, the scheme of two-center interference is constructed based on molecular photoionization through an electric dipole transition. Since electric quadrupole contributions are typically two to three orders of magnitude smaller than dipole contributions, the structure of two-center interference originating from EWPs generated by multipolar interactions has not been fully elucidated.

In this paper, we numerically solve the two-dimensional (2D) time-dependent Schrödinger equation (TDSE) beyond the dipole approximation and employ perturbation theory to demonstrate that the two-center interference structure induced by the electric quadrupole transition in the one-photon ionization of H_2^+ can be discerned from the asymmetric photoelectron angular distribution along the laser propagation direction. These simulations are performed with the fixed nuclei approximation. The EWPs ionized due to the electric quadrupole transition from the two nuclei of the molecule exhibit an additional phase difference, resulting in a distinctive two-center interference structure compared to the electric dipole transition. Interestingly, this approach offers a different perspective on revealing the nondipole effect-induced shifts in two-center interference fringes observed in recent experiments [42]. Furthermore, a feasible experiment scheme based on the technique of reconstruction of attosecond beating by interference of two-photon transitions (RABBIT) is proposed to reveal the two-center interference structure induced by the electric quadrupole transition. The electric quadrupole transition induced two-center interference structure results in a phase jump of the RABBIT phase, from which the interference minima can be traced.

II. NUMERICAL METHODS

We numerically solve the two-dimensional time-dependent Schrödinger equation with the fixed nuclei approximation to investigate the nondipole effect in H_2^+ photoionization.

In the velocity gauge, the dynamics of the molecule-field interaction is determined by the Hamiltonian (atomic units are used unless otherwise stated)

$$H = \frac{1}{2}[\mathbf{p} + \mathbf{A}(\mathbf{r}, t)]^2 + V(r). \quad (1)$$

We consider a laser pulse with vector potential $\mathbf{A}(\mathbf{r}, t) = \mathbf{A}(t - \hat{\mathbf{k}} \cdot \mathbf{r}/c)$, where c is the speed of light. Expanding the vector potential in $1/c$ and inserting the expansion into Eq. (1), while neglecting terms proportional to $1/c^2$, leads to

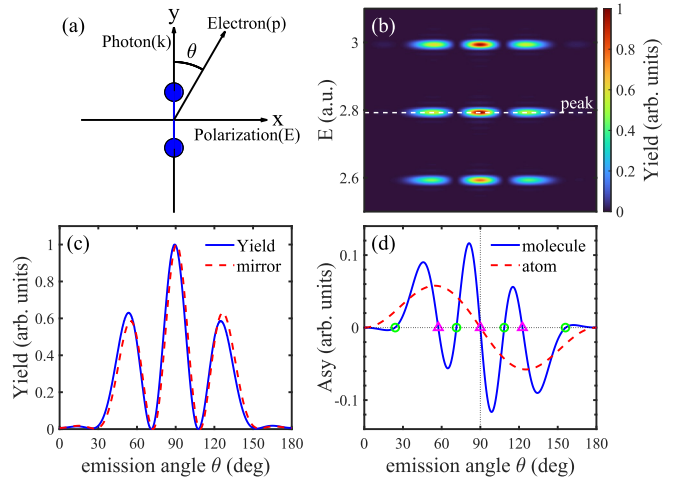


FIG. 1. (a) Illustration of the coordinates in our simulation: The nuclei of H_2^+ are fixed along the y axis. The laser pulse is linearly polarized along the \hat{x} axis and propagates along the \hat{y} axis. θ denotes the electron emission direction relative to the light propagation direction. (b) Angle-resolved PEMD for H_2^+ photoionization by the XUV attosecond pulse train alone for $R = 4$ a.u. (c) The photoelectron angular distribution for $E = 2.8$ a.u., marked by the white dashed line in (b). Additionally, the mirror image, i.e., $\text{Yield}(\pi - \theta)$, is shown (red dashed line) to illustrate the asymmetry. (d) The asymmetric parameter Asy as a function of the emission angle θ for molecular (blue solid line) and atomic (red dashed line) photoionization.

the Hamiltonian

$$H = \frac{1}{2}[\mathbf{p} + \mathbf{A}(t)]^2 + \frac{\hat{\mathbf{k}} \cdot \mathbf{r}}{c}[\mathbf{p} + \mathbf{A}(t)] \cdot \mathbf{E}(t) + V(r), \quad (2)$$

where $\hat{\mathbf{k}} = \mathbf{k}/k$ is the unit vector the laser field propagation direction with photon momentum \mathbf{k} and $\mathbf{E}(t)$ is the laser electric field. Applying a unitary transformation [48] to the Hamiltonian in Eq. (2), we obtain the transformed Hamiltonian

$$H = \frac{1}{2} \left[\mathbf{p} + \mathbf{A}(t) + \frac{\hat{\mathbf{k}}}{c} \left(\mathbf{p} \cdot \mathbf{A}(t) + \frac{1}{2} \mathbf{A}^2(t) \right) \right]^2 + V \left(\mathbf{r} - \frac{\hat{\mathbf{k}} \cdot \mathbf{r}}{c} \mathbf{A}(t) \right). \quad (3)$$

Here, the nondipole effect is described by the third term in the square brackets and the shifted potential. $V(\mathbf{r})$ is the Coulomb potential of H_2^+ , written as

$$V(\mathbf{r}) = -\frac{1}{\sqrt{|\mathbf{r} - \mathbf{R}/2|^2 + a(R)}} - \frac{1}{\sqrt{|\mathbf{r} + \mathbf{R}/2|^2 + a(R)}}, \quad (4)$$

where $\mathbf{R} = R\hat{e}_y$ with internuclear distance R , and $a(R)$ is a soft-core parameter tuned to match the ground state energy of H_2^+ . In our calculation, the laser pulse propagates along the y axis and is linearly polarized along the x axis, as shown in Fig. 1(a) and the laser vector potential is defined as $\mathbf{A}(t) = [A_{\text{APT}}(t) + A_{\text{UV}}(t)]\hat{e}_x$, where $A_{\text{APT}}(t)$ ($A_{\text{UV}}(t)$) is the vector potential of the attosecond pulse train (APT) (UV field). Thus,

$A_{\text{APT}}(t)$ is written as

$$A_{\text{APT}}(t) = \sum_{n=-8}^8 A_n \exp \left[-2 \ln 2 \left(\frac{t - nT/2}{0.05T} \right)^2 \right] \times (-1)^n \cos[N_c \omega(t - nT/2)]. \quad (5)$$

Here, $A_n = A_a \exp[-2 \ln 2(t/4T)^2]$, $N_c = 29$, $\omega = 0.1$ a.u., $T = 2\pi/\omega$ are the APT envelope, the center harmonic order, the laser frequency, and the optical cycle, respectively. Likewise, $A_{\text{UV}}(t)$ becomes

$$A_{\text{UV}}(t) = A_0 \cos^2 \left(\frac{\pi(t - \tau)}{NT} \right) \cos[\omega(t - \tau)], \quad (6)$$

where A_0 and $N = 16$ are the vector potential peak amplitude and the number of the optical cycles of the UV pulse, respectively. τ is the time delay between the APT and UV laser pulses. In our calculation, the intensities of APT and UV pulses are 5×10^{13} and 5×10^{11} W/cm², respectively.

In our simulation, the 2D-TDSE with the Hamiltonian shown in Eq. (3) is numerically solved using the standard Fourier split-operator method [49] with a time step of $\Delta t = 0.005$ a.u. The numerical grid size is 205 a.u. in the x and y directions with spacings of $\Delta x = \Delta y = 0.2$ a.u. The initial stationary wave functions are obtained using the imaginary-time method [50]. The wave function $\Psi(\mathbf{r}, t)$ is split into inner and outer parts using a mask function with a radius of 90 a.u. In the inner space, the wave function propagates under the full Hamiltonian, while in the outer space, it analytically propagates under the nondipole-corrected Volkov Hamiltonian [51]. At the end of the laser pulse, the wave function propagates under the field-free Hamiltonian for an additional four optical cycles to collect the ‘‘slow’’ electrons. The photoelectron momentum distribution (PEMD) is obtained at the final time from the asymptotic grid with a resolution of $\Delta p_x = \Delta p_y = 0.005$ a.u. The simulation’s convergence has been confirmed with shorter time steps and finer spatial grids.

III. RESULTS AND DISCUSSIONS

A. One-photon ionization

Figure 1(b) shows the angle-resolved photoelectron spectrum for the photoionization of H_2^+ by the APT alone. The multiplex structure at different energies in the spectrum originates from one-photon ionization by absorbing different orders of harmonics. The nodal structure in the peaks arises from the two-center interference in molecular ionization. To highlight the two-center interference structure more clearly, the angular distribution at $E = 2.8$ a.u. [marked by the white dashed line in Fig. 1(b)] is displayed in Fig. 1(c). In the dipole approximation, the angular distribution is symmetric about the polarization direction, i.e., $\theta = 90^\circ$. Due to nondipole interactions, the symmetry is broken, as indicated by the comparison between the distribution (blue solid line) and its mirror image (red dashed line) in Fig. 1(c). In previous work [42], the zeptosecond birth time delay has been extracted from the shift of the interference maxima around $\theta = 90^\circ$. In addition to this interference fringe shift, the angular distribution shows yield asymmetry. To quantify this asymmetry, we define an

asymmetric parameter as

$$\text{Asy}(E, \theta) = \frac{\text{Yield}(E, \theta) - \text{Yield}(E, \pi - \theta)}{\text{Max}[\text{Yield}(E, \theta)]}. \quad (7)$$

Here, $\text{Yield}(E, \theta)$ denotes the photoelectron yield at the emission angle θ and the photoelectron energy E . The asymmetric parameter for molecular photoionization (blue solid line) at $E = 2.8$ a.u. is shown in Fig. 1(d). Similar to the photoelectron yield shown in Fig. 1(c), the asymmetric parameter also oscillates with θ around zero. The red dashed line in Fig. 1(d) represents the results for a model atom with the binding energy equivalent to H_2^+ . The comparison between atomic and molecular results indicates that the oscillation of the asymmetric parameter for molecular ionization originates from its two-center structure. More specifically, the zero points marked by circles correspond to the interference minima of the photoelectron yield, as shown in Fig. 1(c). Meanwhile, the zero points marked by triangles do not have counterparts in the photoelectron yield distribution. In this work, we focus on this phenomenon.

To elucidate the origin of the asymmetric parameter behavior in molecular ionization, we first separate the contributions of the photoelectron yield due to multipolar interactions. Applying the Powers-Zienau-Wolley gauge transformation [52,53] to Eq. (2), the Hamiltonian transforms as follows,

$$H = \underbrace{\frac{\mathbf{p}^2}{2} + V(\mathbf{r}) + \mathbf{r} \cdot \mathbf{E}(t)}_{H_D} - \underbrace{\frac{1}{2c}(\hat{\mathbf{k}} \cdot \mathbf{r}) \left[\mathbf{r} \cdot \frac{\partial \mathbf{E}(t)}{\partial t} \right]}_{E2 \text{ term}} + \underbrace{\frac{1}{2c} \mathbf{L} \cdot [\hat{\mathbf{k}} \times \mathbf{E}(t)]}_{B1 \text{ term}}, \quad (8)$$

where $\mathbf{L} = \mathbf{r} \times \mathbf{p}$ represents the angular momentum operator. This Hamiltonian in the multipolar gauge provides a transparent physical insight by separating the electric quadrupole ($E2$) and magnetic dipole ($B1$) effects in nondipole interactions. In this case, H_D denotes the Hamiltonian under the dipole approximation. The last two terms describe the electric quadrupole and magnetic dipole interactions. Previous work [36] has shown that the magnetic dipole effect is one order of magnitude smaller than the electric quadrupole contribution in one-photon ionization of the molecule, considering the internuclear distance and the photoelectron energy range considered in our study. Thus, the magnetic dipole effect can be safely ignored. Therefore, the photoelectron yield can be expressed as

$$\begin{aligned} \text{Yield} &= |T_D + T_{E2}|^2 \\ &= |T_D|^2 + T_D T_{E2}^* + T_D^* T_{E2} + O\left(\frac{1}{c^2}\right), \end{aligned} \quad (9)$$

where T_D and T_{E2} are the transition amplitudes of the electric dipole and quadrupole terms, respectively. The electric dipole transition is symmetric along the laser propagation direction, i.e., $T_D(\theta) = T_D(\pi - \theta)$. Therefore, the asymmetry parameter defined in Eq. (7) can be written as

$$\text{Asy} \propto T_D T_{E2}^* + T_D^* T_{E2}, \quad (10)$$

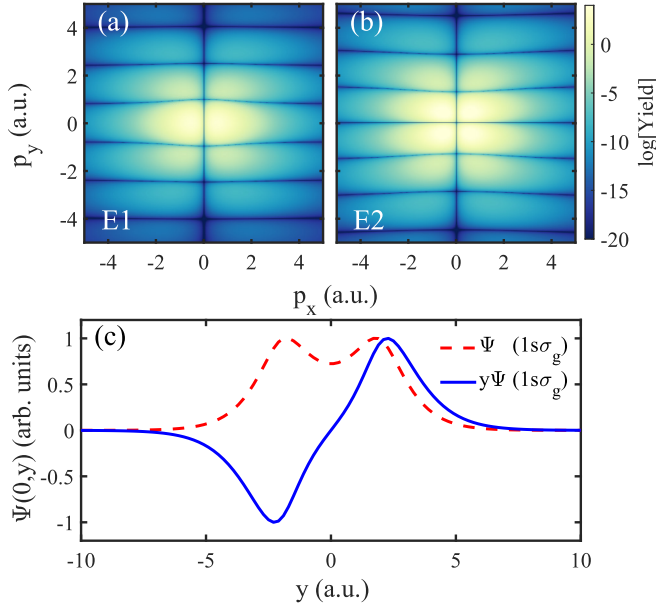


FIG. 2. (a) Numerical results for the modulus of the electric dipole transition matrix element $|\mathcal{T}_D|^2$ (logarithmic color scale) are presented at an internuclear distance of 4 a.u. (b) Similar results as in (a), but for the electric quadrupole transition matrix element $|\mathcal{T}_{E2}|^2$ (logarithmic color scale) at an internuclear distance of 4 a.u. (c) Cut of the initial-state wave function for the $1s\sigma_g$ state is shown with the red dashed line at $x = 0$. The blue solid line represents $y\Psi$ for the $1s\sigma_g$ state at $x = 0$. Both wave functions are normalized by their maximum values.

which represents the interference between the electric dipole and quadrupole transitions.

As indicated by Eq. (8), in the first-order perturbation theory (PT), the electric dipole and quadrupole transition amplitudes in the ionization of H_2^+ are given by

$$T_D = -i \int_{-\infty}^{+\infty} dt E(t) e^{-i(E_f - E_i)t} \langle \psi_f | x | \psi_i \rangle, \quad (11)$$

and

$$T_{E2} = i \int_{-\infty}^{+\infty} dt \frac{1}{2c} \dot{E}(t) e^{-i(E_f - E_i)t} \langle \psi_f | xy | \psi_i \rangle, \quad (12)$$

respectively. Here, ψ_i and ψ_f are the initial and final states with corresponding energies E_i and E_f . The interference structure induced by the two-center structure of the molecule is determined by the transition matrix elements, $\mathcal{T}_D = \langle \psi_f | x | \psi_i \rangle$ and $\mathcal{T}_{E2} = \langle \psi_f | xy | \psi_i \rangle$. By approximately setting the final state as a plane wave $\langle \mathbf{r} | \psi_f \rangle = e^{i\mathbf{p}\cdot\mathbf{r}}$, the squared moduli of transition matrix elements for the electric dipole $|\mathcal{T}_D|^2$ and quadrupole $|\mathcal{T}_{E2}|^2$ are obtained, as shown in Figs. 2(a) and 2(b), respectively. The horizontal fringes originate from the two-center structure of the molecule. For the electric dipole ($E1$) transition, the well-known two-center interference pattern is modulated by the factor $\cos^2(\mathbf{p} \cdot \mathbf{R}/2)$, as illustrated in Fig. 2(a). The interference minima are determined by $\cos^2(\mathbf{p} \cdot \mathbf{R}/2) = 0$, i.e., $p_y = (2n + 1)\pi/R$, where n is an integer. This interference structure is manifested in the photoelectron yield distribution as shown in Figs. 1(b) and 1(c). For the electric quadrupole ($E2$) transition, as shown in Fig. 2(b), the

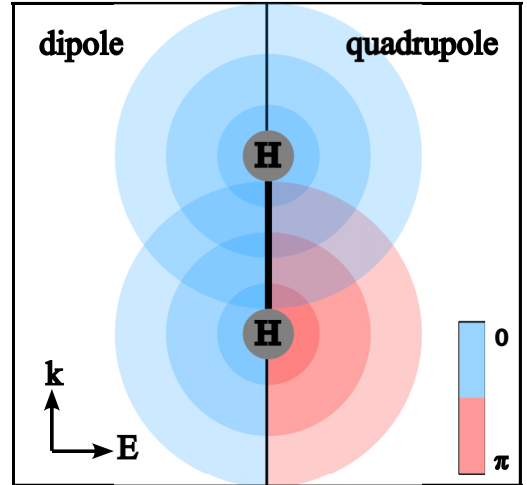


FIG. 3. Illustration of the phase of the electron wave packets (EWPs) generated by the electric dipole and quadrupole transitions from two nuclei. The left plane represents the results for the electric dipole transition, while the right plane represents the results for the quadrupole transition.

interference fringes are almost out of phase with those in the dipole transition. The interference minima are approximately located at $p_y = 2n\pi/R$. The symmetry difference between $E1$ and $E2$ transitions is due to the operator y in the $E2$ elements, \mathcal{T}_D and \mathcal{T}_{E2} . In Fig. 2(c), we display the cuts of the initial state (red dashed line) and $y\Psi$ (blue solid line) at $x = 0$. The wave function of the $1s\sigma_g$ state is symmetric about $y = 0$, while $y\Psi$ is antisymmetric. Therefore, the $E2$ transition has an additional phase of π compared to the $E1$ transition due to the y operator. Thus, the two-center interference induced by the $E2$ transition can be approximately expressed as $|\mathcal{T}_{E2}|^2 \propto \sin^2(\mathbf{p} \cdot \mathbf{R}/2)$. This term qualitatively coincides with the numerical results shown in Fig. 2(b).

In addition, this different interference structure can also be understood from the phase of the electron wave packets (EWPs), as illustrated in Fig. 3. For ionization from the ground state of H_2^+ , the phases of the EWPs generated from the two nuclei by the $E1$ transition are the same, resulting in the interference structure determined by $\cos^2(\mathbf{p} \cdot \mathbf{R}/2)$. In contrast, for the $E2$ transition, the phases of the EWPs generated from the two nuclei have a π difference, leading to an interference structure determined by $\sin^2(\mathbf{p} \cdot \mathbf{R}/2)$.

In previous works, this two-center interference structure induced by the $E2$ transition has not been observed, primarily due to the challenge of separating the contribution of the $E2$ transition from the photoelectron momentum distribution (PEMD). Nevertheless, the asymmetric parameter we focus on, representing the interference between $E1$ and $E2$ transitions as shown in Eq. (10), encodes the two-center interference structure induced by the $E2$ transition. As addressed above and implied by Eq. (10), the asymmetric parameter can be rewritten as

$$\begin{aligned} \text{Asy} &= 2T_D T_{E2}^* + 2T_D^* T_{E2} \\ &\propto \cos(\mathbf{p} \cdot \mathbf{R}/2) \sin(\mathbf{p} \cdot \mathbf{R}/2). \end{aligned} \quad (13)$$

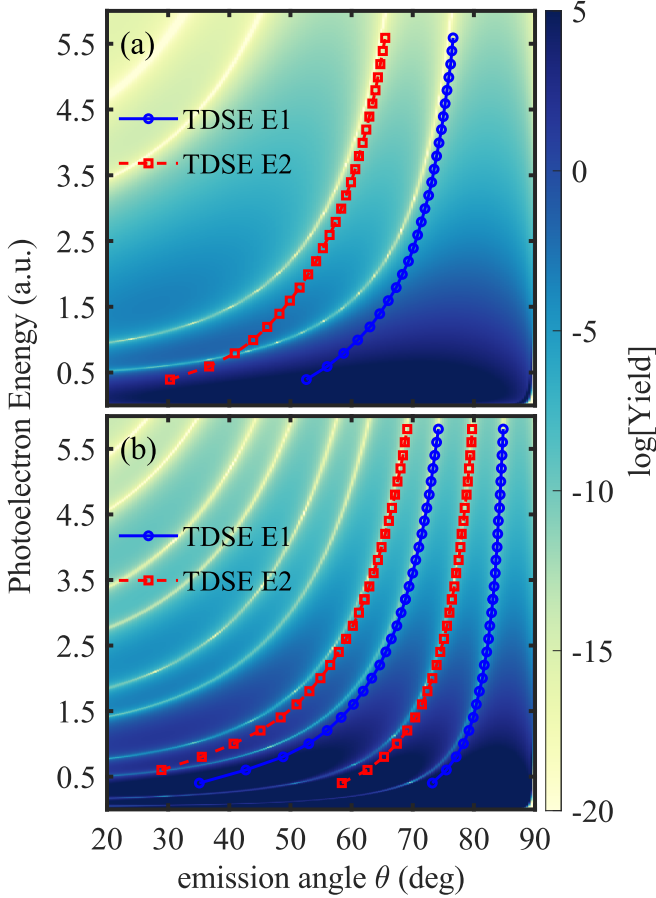


FIG. 4. (a) Comparison between interference minima extracted from the asymmetric parameters obtained by numerically solving the TDSE and perturbation theory. The red dashed line and blue solid line represent the interference minima induced by electric dipole and quadrupole transitions extracted from TDSE results, respectively. The background interference structure is obtained from perturbation theory. The internuclear distance R is 4 a.u. (b) Same as (a) but for $R = 10$ a.u.

This last expression indicates that the oscillation observed in the asymmetric parameter shown in Fig. 1(d) encodes information about the two-center interference of $E1$ and $E2$ transitions. The zero points of the asymmetric parameter represent the interference minima of the two-center interference structure induced by the $E1$ and $E2$ transitions, respectively, i.e., $\cos(\mathbf{p} \cdot \mathbf{R}/2) = 0$ corresponds to the zero points marked by circles in Fig. 1(d) and $\sin(\mathbf{p} \cdot \mathbf{R}/2) = 0$ corresponds to the zero points marked by triangles in Fig. 1(d). This means that the two-center interference structure induced by the $E1$ and $E2$ transitions can be revealed from this asymmetric parameter. Figure 4 shows interference minima extracted from the asymmetric parameters obtained by numerically solving the TDSE (lines with symbols) and the results obtained by numerically calculating the modulus of the transition matrix elements $|\mathcal{T}_D \mathcal{T}_{E2}|$. Figures 4(a) and 4(b) are the results for $R = 4$ and 10 a.u., respectively. Obviously, these results agree well with each other. The deviation appearing in the low-energy region is due to the Coulomb effect on the continuous states, which is not accounted for in the model given by

Eq. (13). Note that we have also calculated the results for other internuclear distances. The conclusion holds for different internuclear distances.

Moreover, the interference scheme discussed above provides a different perspective on revealing the nondipole effect in one-photon molecular ionization, such as the shift of the two-center interference fringes. Recent work [42] has explained this shift as due to the finite speed of light. As indicated by Eq. (9) and the analysis above, the photoelectron yield can be expressed as

$$\text{Yield} = |\mathcal{A}_D(\theta) \cos(\mathbf{p} \cdot \mathbf{R}/2) + \mathcal{A}_{E2}(\theta) \sin(\mathbf{p} \cdot \mathbf{R}/2)|^2 \propto |\cos[\mathbf{p} \cdot \mathbf{R}/2 + \delta(\theta)]|^2, \quad (14)$$

with $\delta(\theta) = \arctan[\mathcal{A}_{E2}(\theta)/\mathcal{A}_D(\theta)]$. Here, \mathcal{A}_D and \mathcal{A}_{E2} represent the amplitudes of the $E1$ and $E2$ transitions, respectively. This implies that the shift of the two-center interference fringes originates from the interference of the EWPs generated by the $E1$ and $E2$ transitions. The amount of the shift is determined by the ratio of the amplitudes of the $E1$ and $E2$ transitions. Recent theoretical works have demonstrated that the fringe shift is different at the interference minima and maxima [43,44]. As indicated by Eq. (14), this phenomenon originates from the emission-angle dependence of the phase shift δ . It implies that the emission-angle-dependent ratio of the amplitudes of the $E1$ and $E2$ transitions can be revealed from the emission-angle-dependent δ .

B. Two-photon ionization in the RABBIT scheme

In experiments, due to the imperfect homogeneity of the detector, measuring the asymmetric parameter defined in Eq. (7) directly is challenging. Recent work [17], however, has shown that the RABBIT scheme can reveal the asymmetric photoelectron yield induced by the $E2$ transition in atomic ionization. Here, we apply this method to explore the two-center interference structure induced by the $E2$ transition in the photoionization of H_2^+ .

Figure 5(a) displays the delay- and angle-resolved photoelectron spectrum obtained by numerically solving the TDSE. The photoelectron energy is 1.89 a.u., corresponding to sideband (SB) 30. The dashed line in Fig. 5(a) represents the two-center interference minima induced by the dipole transition.

To reveal the asymmetry of the photoelectron yield induced by the $E2$ transition, we define the asymmetric parameter as

$$\text{Asy}(E, \theta, \tau) = \frac{I(E, \theta, \tau) - I(E, \pi - \theta, \tau)}{\text{Max}[\text{Yield}(E, \theta)]}, \quad (15)$$

where $I(E, \theta, \tau) = \text{Yield}(E, \theta, \tau) - \overline{\text{Yield}}(E, \theta)$ is the normalized photoelectron distribution, where $\overline{\text{Yield}}(E, \theta)$ is the time-delay averaged photoelectron distribution. This normalized photoelectron distribution eliminates systematic errors due to imperfect detector homogeneity, thereby revealing the subtle asymmetry in the photoelectron angular distribution induced by the $E2$ transition [17]. The delay- and angle-resolved asymmetric parameter is shown in Fig. 5(b), oscillating with the time delay between the XUV and UV fields,

$$\text{Asy}(\tau, \theta) \propto \cos[2\omega\tau + \Delta\phi_{\text{Asy}}(\theta)]. \quad (16)$$

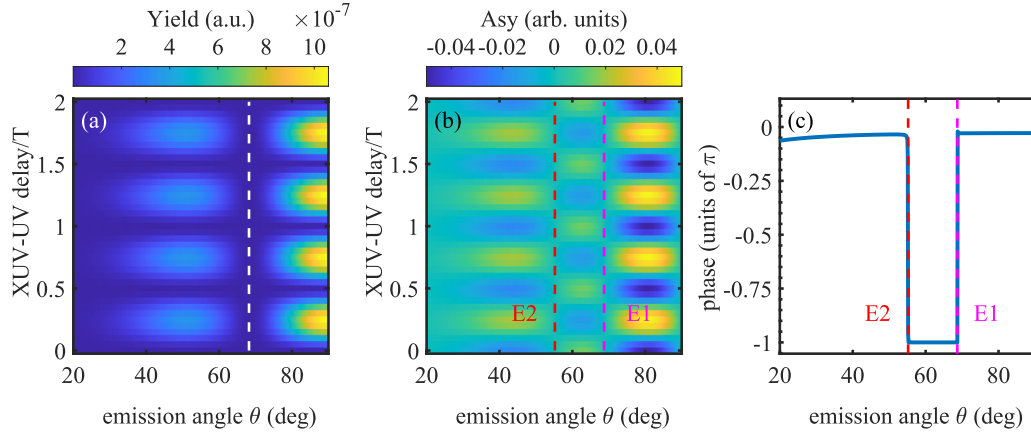


FIG. 5. (a) The delay- and angle-resolved photoelectron spectrum obtained by numerically solving the TDSE. The photoelectron energy is 1.89 a.u., corresponding to sideband (SB) 30. The internuclear distance is 4 a.u. (b) The delay- and angle-resolved asymmetric parameter $Asy(\theta, \tau)$ obtained using Eq. (15) with the same energy as in (a). (c) The angular-resolved phase shift of the asymmetric parameter $\Delta\phi_{Asy}(\theta)$ extracted from (b).

The two-node structure is clearly revealed in the angular distribution of the asymmetric parameter, as indicated by the dashed lines in Fig. 5(b). As discussed in Sec. III A, these nodes correspond to the interference minima induced by the $E1$ and $E2$ transitions, respectively. The angular-resolved phase shift of the asymmetric parameter $\Delta\phi_{Asy}(\theta)$ is extracted by fitting the asymmetric parameter as a function of the XUV-UV time delay, as shown in Fig. 5(c). The two-center interference induced by the $E1$ and $E2$ transitions introduces a phase jump in the asymmetric parameter, indicating that the interference structure induced by the $E2$ transition can be revealed through this phase shift. As the emission angle increases, this rapidly changing phase shift trend becomes more easily measurable in experiments, which provides an accurate determination of the two-center interference structure induced by the electric quadrupole effect.

In experiments, challenges such as molecular alignment and nonfixed nuclei can be addressed using techniques such as cold target recoil ion momentum spectroscopy (COLTRIMS) [22,54]. By combining the RABBIT scheme with COLTRIMS, the asymmetric parameters can be measured experimentally [17]. Furthermore, the two-center interference induced by the $E2$ transition exists not only in H_2^+ but also in more general diatomic molecules such as N_2 and O_2 . Therefore, our theoretical predictions have great potential to be observed using current experimental approaches.

IV. CONCLUSION

In summary, by numerically solving the TDSE beyond the dipole approximation and employing perturbation theory, we demonstrate that the two-center interference structure in H_2^+ photoionization induced by the $E2$ transition can be

discerned from the asymmetric photoelectron yield along the laser propagation direction. Unlike the $E1$ transition, the electron wave packets (EWPs) emitted from the two nuclei of the molecule via the $E2$ transition exhibit an additional phase difference, resulting in a distinct interference structure compared to the dipole case. The photoelectron momentum distribution (PEMD) reflects the interference between the $E1$ and $E2$ transitions. Our approach provides a different perspective for unveiling nondipole effects in molecular photoionization. Furthermore, we propose a feasible experimental method based on the RABBIT technique to reveal the two-center interference induced by the $E2$ transition. The present study enhances our understanding of nondipole effects in molecular photoionization.

ACKNOWLEDGMENTS

This work was supported by National Key Research and Development Program of China (Grant No. 2019YFA0308300), National Natural Science Foundation of China (Grants No. 12374264 and No. 12174133), and the Open Project Fund from Guangdong Provincial Key Laboratory of Materials and Technology for Energy Conversion, Guangdong Technion-Israel Institute of Technology (Grant No. MATEC2023KF001). Numerical simulations presented in this paper were completed in the High Performance Computing Center in SCTS/CGCL. M.F.C. acknowledges the National Key Research and Development Program of China (Grant No. 2023YFA1407100), the Guangdong Province Science and Technology Major Project (Future functional materials under extreme conditions - 2021B0301030005) and the Guangdong Natural Science Foundation (General Program Project No. 2023A1515010871).

[1] H. R. Reiss, Limits on tunneling theories of strong-field ionization, *Phys. Rev. Lett.* **101**, 043002 (2008).

[2] E. Stambulchik and Y. Maron, Zeeman effect induced by intense laser light, *Phys. Rev. Lett.* **113**, 083002 (2014).

- [3] J. Liang, Y. Zhou, W.-C. Jiang, M. Yu, M. Li, and P. Lu, Zeeman effect in strong-field ionization, *Phys. Rev. A* **105**, 043112 (2022).
- [4] A. Ludwig, J. Maurer, B. W. Mayer, C. R. Phillips, L. Gallmann, and U. Keller, Breakdown of the dipole approximation in strong-field ionization, *Phys. Rev. Lett.* **113**, 243001 (2014).
- [5] K. Lin, S. Brennecke, H. C. Ni, X. Chen, A. Hartung, D. Trabert, K. Fehre, J. Rist, X. M. Tong, J. Burgdörfer, L. Ph. H. Schmidt, M. S. Schöffler, T. Jahnke, M. Kunitski, F. He, M. Lein, S. Eckart, and R. Dörner, Magnetic-field effect in high-order above-threshold ionization, *Phys. Rev. Lett.* **128**, 023201 (2022).
- [6] K. Lin, X. Chen, S. Eckart, H. Jiang, A. Hartung, D. Trabert, K. Fehre, J. Rist, L. Ph. H. Schmidt, M. S. Schöffler, T. Jahnke, M. Kunitski, F. He, and R. Dörner, Magnetic-field effect as a tool to investigate electron correlation in strong-field ionization, *Phys. Rev. Lett.* **128**, 113201 (2022).
- [7] J. Liang, Y. Zhou, Y. Liao, W.-C. Jiang, M. Li, and P. Lu, Direct visualization of deforming atomic wavefunction in ultraintense high-frequency laser pulses, *Ultrafast Sci.* **2022**, 9842716 (2022).
- [8] J. Xu, J. Liang, X. Ma, K. Liu, Y. Li, C. Cao, M. Li, B. Yu, Y. Zhou, and P. Lu, Pronounced momentum shift against the radiation pressure in strong-field sequential double ionization, *Phys. Rev. A* **108**, 043103 (2023).
- [9] B. Willenberg, J. Maurer, B. W. Mayer, and U. Keller, Subcycle time resolution of multi-photon momentum transfer in strong-field ionization, *Nat. Commun.* **10**, 5548 (2019).
- [10] A. Hartung, S. Eckart, S. Brennecke, J. Rist, D. Trabert, K. Fehre, M. Richter, H. Sann, S. Zeller, K. Henrichs, G. Kastirke, J. Hoehl, A. Kalinin, M. S. Schöffler, T. Jahnke, L. Ph. H. Schmidt, M. Lein, M. Kunitski, and R. Dörner, Magnetic fields alter strong-field ionization, *Nat. Phys.* **15**, 1222 (2019).
- [11] H. Ni, S. Brennecke, X. Gao, P.-L. He, S. Donsa, I. Březinová, F. He, J. Wu, M. Lein, X.-M. Tong, and J. Burgdörfer, Theory of subcycle linear momentum transfer in strong-field tunneling ionization, *Phys. Rev. Lett.* **125**, 073202 (2020).
- [12] J. Liang, W. Wang, K. Liu, W.-C. Jiang, L. Guo, Y. Zhou, and P. Lu, Time resolving the photoelectron motion driven by the magnetic component of a laser field, *Phys. Rev. A* **109**, 023102 (2024).
- [13] M. O. Krause, Photo-ionization of krypton between 300 and 1500 eV. Relative subshell cross sections and angular distributions of photoelectrons, *Phys. Rev.* **177**, 151 (1969).
- [14] F. Wuilleumier and M. O. Krause, Photoionization of neon between 100 and 2000 eV: Single and multiple processes, angular distributions, and subshell cross sections, *Phys. Rev. A* **10**, 242 (1974).
- [15] B. Krässig, M. Jung, D. S. Gemmell, E. P. Kanter, T. LeBrun, S. H. Southworth, and L. Young, Nondipolar asymmetries of photoelectron angular distributions, *Phys. Rev. Lett.* **75**, 4736 (1995).
- [16] J. W. Cooper, Photoelectron-angular-distribution parameters for rare-gas subshells, *Phys. Rev. A* **47**, 1841 (1993).
- [17] J. Liang, M. Han, Y. Liao, J.-B. Ji, C. S. Leung, W.-C. Jiang, K. Ueda, Y. Zhou, P. Lu, and H. J. Wörner, Attosecond-resolved non-dipole photoionization dynamics, *Nat. Photonics* **18**, 311 (2024).
- [18] B. Krässig, E. P. Kanter, S. H. Southworth, R. Guillemin, O. Hemmers, D. W. Lindle, R. Wehlitz, and N. L. S. Martin, Photoexcitation of a dipole-forbidden resonance in helium, *Phys. Rev. Lett.* **88**, 203002 (2002).
- [19] M. Ilchen, G. Hartmann, E. V. Gryzlova, A. Achner, E. Allaria, A. Beckmann, M. Braune, J. Buck, C. Callegari, R. N. Coffee, R. Cucini, M. Danailov, A. De Fanis, A. Demidovich, E. Ferrari, P. Finetti, L. Glaser, A. Knie, A. O. Lindahl, O. Plekan, N. Mahne, T. Mazza, L. Raimondi, E. Roussel, F. Scholz, J. Seltmann, I. Shevchuk, C. Svetina, P. Walter, M. Zangrando, J. Viehhaus, A. N. Grum-Grzhimailo, and M. Meyer, Symmetry breakdown of electron emission in extreme ultraviolet photoionization of argon, *Nat. Commun.* **9**, 4659 (2018).
- [20] F. Lépine, S. Zamith, A. de Snaijer, Ch. Bordas, and M. J. J. Vrakking, Observation of large quadrupolar effects in a slow photoelectron imaging experiment, *Phys. Rev. Lett.* **93**, 233003 (2004).
- [21] S. Chelkowski, A. D. Bandrauk, and P. B. Corkum, Photon momentum sharing between an electron and an ion in photoionization: From one-photon (photoelectric effect) to multiphoton absorption, *Phys. Rev. Lett.* **113**, 263005 (2014).
- [22] S. Grundmann, M. Kircher, I. Vela-Perez, G. Nalin, D. Trabert, N. Anders, N. Melzer, J. Rist, A. Pier, N. Strenger, J. Siebert, P. V. Demekhin, L. Ph. H. Schmidt, F. Trinter, M. S. Schöffler, T. Jahnke, and R. Dörner, Observation of photoion backward emission in photoionization of He and N_2 , *Phys. Rev. Lett.* **124**, 233201 (2020).
- [23] H. D. Cohen and U. Fano, Interference in the photo-ionization of molecules, *Phys. Rev.* **150**, 30 (1966).
- [24] D. Akoury, K. Kreidi, T. Jahnke, T. Weber, A. Staudte, M. Schöffler, N. Neumann, J. Titze, L. P. H. Schmidt, A. Czasch, O. Jagutzki, R. A. C. Fraga, R. E. Grisenti, R. D. Muiño, N. A. Cherepkov, S. K. Semenov, P. Ranitovic, C. L. Cocke, T. Osipov, H. Adaniya, J. C. Thompson, M. H. Prior, A. Belkacem, A. L. Landers, H. Schmidt-Böcking, and R. Dörner, The simplest double slit: Interference and entanglement in double photoionization of H_2 , *Science* **318**, 949 (2007).
- [25] M. S. Schöffler, K. Kreidi, D. Akoury, T. Jahnke, A. Staudte, N. Neumann, J. Titze, L. P. H. Schmidt, A. Czasch, O. Jagutzki, R. A. Costa Fraga, R. E. Grisenti, M. Smolarski, P. Ranitovic, C. L. Cocke, T. Osipov, H. Adaniya, S. Lee, J. C. Thompson, M. H. Prior, A. Belkacem, T. Weber, A. Landers, H. Schmidt-Böcking, and R. Dörner, Photo-double-ionization of H_2 : Two-center interference and its dependence on the internuclear distance, *Phys. Rev. A* **78**, 013414 (2008).
- [26] M. Waitz, D. Metz, J. Lower, C. Schober, M. Keiling, M. Pitzer, K. Mertens, M. Martins, J. Viehhaus, S. Klumpp, T. Weber, H. Schmidt-Böcking, L. Ph. H. Schmidt, F. Morales, S. Miyabe, T. N. Rescigno, C. W. McCurdy, F. Martín, J. B. Williams, M. S. Schöffler, T. Jahnke, and R. Dörner, Two-particle interference of electron pairs on a molecular level, *Phys. Rev. Lett.* **117**, 083002 (2016).
- [27] D. Rolles, M. Braune, S. Cvejanović, O. Geßner, R. Hentges, S. Korica, B. Langer, T. Lischke, G. Prümper, A. Reinköster, J. Viehhaus, B. Zimmermann, V. McKoy, and U. Becker, Isotope-induced partial localization of core electrons in the homonuclear molecule N_2 , *Nature (London)* **437**, 711 (2005).
- [28] B. Zimmermann, D. Rolles, B. Langer, R. Hentges, M. Braune, S. Cvejanovic, O. Geßner, F. Heiser, S. Korica, T. Lischke, A. Reinköster, J. Viehhaus, R. Dörner, V. McKoy, and U. Becker,

- Localization and loss of coherence in molecular double-slit experiments, *Nat. Phys.* **4**, 649 (2008).
- [29] M. S. Schöffler, J. Titze, N. Petridis, T. Jahnke, K. Cole, L. Ph. H. Schmidt, A. Czasch, D. Akoury, O. Jagutzki, J. B. Williams, N. A. Cherepkov, S. K. Semenov, C. W. McCurdy, T. N. Rescigno, C. L. Cocke, T. Osipov, S. Lee, M. H. Prior, A. Belkacem, A. L. Landers, H. Schmidt-Böcking, Th. Weber, and R. Dörner, Ultrafast probing of core hole localization in N_2 , *Science* **320**, 920 (2008).
- [30] C. Zhang, T. Feng, N. Raabe, and H. Rottke, Strong-field ionization of xenon dimers: The effect of two-equivalent-center interference and of driving ionic transitions, *Phys. Rev. A* **97**, 023417 (2018).
- [31] M. Kunitski, N. Eicke, P. Huber, J. Köhler, S. Zeller, J. Voigtsberger, N. Schlott, K. Henrichs, H. Sann, F. Trinter, L. Ph. H. Schmidt, A. Kalinin, M. S. Schöffler, T. Jahnke, M. Lein, and R. Dörner, Double-slit photoelectron interference in strong-field ionization of the neon dimer, *Nat. Commun.* **10**, 1 (2019).
- [32] S. Brennecke and M. Lein, High-order above-threshold ionization beyond the electric dipole approximation: Dependence on the atomic and molecular structure, *Phys. Rev. A* **98**, 063414 (2018).
- [33] A. D. Bandrauk and H. Z. Lu, Molecules in intense laser fields: Beyond the dipole approximation, *Phys. Rev. A* **73**, 013412 (2006).
- [34] D. Lao, P.-L. He, and F. He, Longitudinal photoelectron momentum shifts induced by absorbing a single XUV photon in diatomic molecules, *Phys. Rev. A* **93**, 063403 (2016).
- [35] S. Chelkowski and A. D. Bandrauk, Photon-momentum transfer in molecular photoionization, *Phys. Rev. A* **97**, 053401 (2018).
- [36] H. Liang, M.-X. Wang, X.-R. Xiao, Q. Gong, and L.-Y. Peng, Photon-momentum transfer in diatomic molecules: An *ab initio* study, *Phys. Rev. A* **98**, 063413 (2018).
- [37] O. Hemmers, H. Wang, P. Focke, I. A. Sellin, D. W. Lindle, J. C. Arce, J. A. Sheehy, and P. W. Langhoff, Large nondipole effects in the angular distributions of K -shell photoelectrons from molecular nitrogen, *Phys. Rev. Lett.* **87**, 273003 (2001).
- [38] R. Guillemin, O. Hemmers, D. W. Lindle, E. Shigemasa, K. Le Guen, D. Ceolin, C. Miron, N. Leclercq, P. Morin, M. Simon, and P. W. Langhoff, Nondipolar electron angular distributions from fixed-in-space molecules, *Phys. Rev. Lett.* **89**, 033002 (2002).
- [39] O. Hemmers, R. Guillemin, D. Rolles, A. Wolska, D. W. Lindle, E. P. Kanter, B. Krässig, S. H. Southworth, R. Wehlitz, B. Zimmermann, V. McKoy, and P. W. Langhoff, Low-energy nondipole effects in molecular nitrogen valence-shell photoionization, *Phys. Rev. Lett.* **97**, 103006 (2006).
- [40] K. Hosaka, J. Adachi, A. V. Golovin, M. Takahashi, T. Teramoto, N. Watanabe, T. Jahnke, T. Weber, M. Schöffler, L. Schmidt, T. Osipov, O. Jagutzki, A. L. Landers, M. H. Prior, H. Schmidt-Böcking, R. Dörner, A. Yagishita, S. K. Semenov, and N. A. Cherepkov, Nondipole effects in the angular distribution of photoelectrons from the $C K$ shell of the Co molecule, *Phys. Rev. A* **73**, 022716 (2006).
- [41] A. N. Grum-Grzhimailo, On the angular distributions in molecular photoionization beyond the dipole approximation, *J. Phys. B: At., Mol. Opt. Phys.* **36**, 2385 (2003).
- [42] S. Grundmann, D. Trabert, K. Fehre, N. Strenger, A. Pier, L. Kaiser, M. Kircher, M. Weller, S. Eckart, L. P. H. Schmidt, F. Trinter, T. Jahnke, M. S. Schöffler, and R. Dörner, Zeptosecond birth time delay in molecular photoionization, *Science* **370**, 339 (2020).
- [43] K. Liu, Y. Hu, Q. Zhang, and P. Lu, Nondipole effects on the double-slit interference in molecular ionization by XUV pulses, *Opt. Express* **29**, 38758 (2021).
- [44] X. Y. Lai, S. P. Xu, S. G. Yu, M. W. Shi, W. Quan, and X. J. Liu, Revealing the wave-function-dependent zeptosecond birth time delay in molecular photoionization with double-slit interference minima, *Phys. Rev. A* **104**, 043105 (2021).
- [45] H. Liang, S. Grundmann, Y.-K. Fang, L. Geng, Q. Gong, and L.-Y. Peng, Nondipole effects in interference patterns of a two-electron wave, *Phys. Rev. A* **104**, L021101 (2021).
- [46] I. A. Ivanov, A. S. Kheifets, and K. T. Kim, Effect of the finite speed of light in ionization of extended molecular systems, *Sci. Rep.* **11**, 21457 (2021).
- [47] Z.-H. Zhang and F. He, Photoionization of H_2^+ beyond the dipole approximation with zeptosecond time resolution, *Phys. Rev. A* **103**, 033112 (2021).
- [48] S. Brennecke and M. Lein, High-order above-threshold ionization beyond the electric dipole approximation, *J. Phys. B: At., Mol. Opt. Phys.* **51**, 094005 (2018).
- [49] M. D. Feit and J. A. Fleck, Solution of the Schrödinger equation by a spectral method II: Vibrational energy levels of triatomic molecules, *J. Chem. Phys.* **78**, 301 (1983).
- [50] M. Protopapas, C. H. Keitel, and P. L. Knight, Atomic physics with super-high intensity lasers, *Rep. Prog. Phys.* **60**, 389 (1997).
- [51] X. M. Tong, K. Hino, and N. Toshima, Phase-dependent atomic ionization in few-cycle intense laser fields, *Phys. Rev. A* **74**, 031405(R) (2006).
- [52] E. A. Power and S. Zienau, Coulomb gauge in non-relativistic quantum electro-dynamics and the shape of spectral lines, *Philos. Trans. R. Soc. London, Ser. A* **251**, 427 (1959).
- [53] R. G. Woolley and C. A. Coulson, Molecular quantum electro-dynamics, *Proc. R. Soc. London, Ser. A* **321**, 557 (1971).
- [54] R. Dörner, V. Mergel, O. Jagutzki, L. Spielberger, J. Ullrich, R. Moshhammer, and H. Schmidt-Böcking, Cold target recoil ion momentum spectroscopy: A ‘momentum microscope’ to view atomic collision dynamics, *Phys. Rep.* **330**, 95 (2000).